THE JOURNAL OF BIOLOGICAL CHEMISTRY VOL. 281, NO. 37, pp. 27613–27620, September 15, 2006


# Predictions of CCR1 Chemokine Receptor Structure and BX 471 Antagonist Binding Followed by Experimental Validation*

Received for publication, February 14, 2006, and in revised form, July 12, 2006 Published, JBC Papers in Press, July 12, 2006, DOI 10.1074/jbc.M601389200

**Nagarajan Vaidehi[‡1], Sabine Schlyer[§], Rene J. Trabanino[‡], Wely B. Floriano[‡], Ravinder Abrol[‡], Shantanu Sharma[‡], Monica Kochanny[§], Sunil Koovakat[§], Laura Dunning[¶], Meina Liang[¶], James M. Fox[‖], Filipa Lopes de Mendonça[‖], James E. Pease[‖], William A. Goddard III[‡], and Richard Horuk[**2]**

*From the Departments of **Immunology, [§]Chemistry, and [¶]Drug Metabolism and Pharmacology, Berlex Biosciences, Richmond, California 94806, the [‡]Materials and Process Simulation Center, California Institute of Technology, Pasadena, California 91125, and the [‖]Leukocyte Biology Section, Imperial College London, London SW7 2AZ, United Kingdom*

**A major challenge in the application of structure-based drug design methods to proteins belonging to the superfamily of G protein-coupled receptors (GPCRs) is the paucity of structural information (1). The 19 chemokine receptors, belonging to the Class A family of GPCRs, are important drug targets not only for autoimmune diseases like multiple sclerosis but also for the blockade of human immunodeficiency virus type 1 entry (2). Using the MembStruk computational method (3), we predicted the three-dimensional structure of the human CCR1 receptor. In addition, we predicted the binding site of the small molecule CCR1 antagonist BX 471, which is currently in Phase II clinical trials (4). Based on the predicted antagonist binding site we designed 17 point mutants of CCR1 to validate the predictions. Subsequent competitive ligand binding and chemotaxis experiments with these mutants gave an excellent correlation to these predictions. In particular, we find that Tyr-113 and Tyr-114 on transmembrane domain 3 and Ile-259 on transmembrane 6 contribute significantly to the binding of BX 471. Finally, we used the predicted and validated structure of CCR1 in a virtual screening validation of the Maybridge data base, seeded with selective CCR1 antagonists. The screen identified 63% of CCR1 antagonists in the top 5% of the hits. Our results indicate that rational drug design for GPCR targets is a feasible approach.**

Chemokines belong to a large family of small, chemotactic cytokines that regulate the trafficking of immune cells (5) by binding to cell surface receptors belonging to the GPCR[3] superfamily (5). CCR1, the first CC chemokine receptor to be identified, responds to a number of ligands, including MIP-1$\alpha$ (CCL3) and RANTES (regulated on activation normal T cell expressed and secreted) (CCL5) (6, 7). The strong association with a wide variety of autoimmune and pro-inflammatory diseases has made the CCR1 protein an attractive therapeutic target, and Berlex has developed a potent, specific, orally available antagonist, BX 471, currently in a Phase II clinical trial (8).

The CCR1 antagonist program that yielded the clinical compound BX 471 followed a traditional drug discovery approach starting with high throughput screening of large compound libraries (9). Although high throughput screening is a main pillar of drug-finding programs in the pharmaceutical industry, it has recently been supplemented by *in silico* methods to maximize the probability of finding attractive novel leads. Structure-based *in silico* approaches have been challenging for GPCRs, because only one experimental GPCR structure, that of bovine rhodopsin, with only ~20% sequence identity to CCR1 (10), has been reported. Recent developments in GPCR structure prediction methods show great potential for structure-based drug design and identifying novel hits from virtual screens (11–15).

In this communication we report a significant test of the computational method MembStruk by predicting the structure of CCR1. Further, we scanned the entire predicted structure using the HierDock computational protocol to identify the binding site of BX 471. Structure and binding site predictions were subsequently tested experimentally using CCR1 point mutants. The MembStruk and HierDock methods were validated for bovine rhodopsin (15) and have been used successfully to predict the structure and ligand binding sites for the $\beta_2$-adrenergic and dopamine $D_2$ receptors (16, 17).

## EXPERIMENTAL PROCEDURES

*Materials*—Unlabeled CCL3 was from Peprotech (London, UK). $^{125}$I-Labeled CCL3 was obtained from Amersham Biosciences. All other reagents were purchased from Sigma-Aldrich and Invitrogen, unless stated otherwise. The monoclonal anti-HA antibody was purchased from Cambridge Bioscience (Cambridge, UK). Fluorescein isothiocyanate-conjugated goat anti-mouse antibody was purchased from DakoCytomation (Ely, UK).

*Generation of HA-tagged CCR1*—The amino terminus of CCR1 was tagged with the HA epitope by PCR using the sense primer 5′-GCGCATAAGCTTGCCACCATGTATCCATATGATGTCCCAGATTATGCCAAAGAATTCGAAACTCCAAACACCACAGAGGA-3′ and the antisense primer SP6 5′-ATTTAGGTGACACTATAGAATAC-3′. The PCR product

* The costs of publication of this article were defrayed in part by the payment of page charges. This article must therefore be hereby marked "*advertisement*" in accordance with 18 U.S.C. Section 1734 solely to indicate this fact.

[1] Present address: Division of Immunology, Beckman Institute of City of Hope, Duarte, CA 91010.

[2] To whom correspondence should be addressed: Berlex Biosciences, Dept. of Immunology, 2600 Hilltop Dr., Richmond, CA 94806. Tel.: 510-669-4625; Fax: 510-669-4244; E-mail: Horuk@pacbell.net.

[3] The abbreviations used are: GPCR, G protein-coupled receptor; HA, hemagglutinin; SPA, scintillation proximity assay; TM, transmembrane.

was then inserted back into pcDNA3.1 at the HindIII and XhoI sites, and its authenticity was verified by fluorescent DNA sequencing of both strands (MWG-Biotech, London, UK).

*Generation of Point Mutants*—Point mutants of CCR1 were generated by PCR using the QuikChange site-directed mutagenesis kit, as previously described (18) (Stratagene), according to the manufacturer's instructions. The fidelity of each construct was verified by DNA sequencing on both strands.

*Tissue Culture*—L1.2 cells were maintained as described previously (19) in suspension at 37 °C with 5% $CO_2$ at a density of no more than $1 \times 10^6$ cells/ml. Cells were transiently transfected by electroporation as described previously (19). In brief, $\sim 1 \times 10^6$ cells per microgram of DNA were electroporated and incubated overnight with medium supplemented with 10 mM sodium butyrate. Cells were harvested and assayed the following day. The HEK293 cell line was obtained from the American Type Culture Collection and was cultured as previously described (9). Human monocytes were isolated as previously described (9).

*CCR1-expressing Cells*—The transfection and selection of HEK293 cells stably expressing human CCR1 was carried out as described previously (9).

*Flow Cytometry*—Approximately $5 \times 10^5$ cells were harvested, washed once with fluorescence-activated cell sorting buffer (0.25% bovine serum albumin and 0.01% $NaN_3$ in phosphate-buffered saline) and then incubated with the primary antibody or the corresponding IgG isotype control for 15 min in a final volume of 100 $\mu$l. Cells were then washed with fluorescence-activated cell sorting buffer and incubated with the fluorescein isothiocyanate-coupled secondary antibody for 15 min in a final volume of 50 $\mu$l. Subsequently, cells were washed with fluorescence-activated cell-sorting buffer and resuspended in a final volume of 400 $\mu$l before being analyzed by flow cytometry as described previously (20). The anti-CCR1 antibody was used at 10 $\mu$g/ml, the anti-hemagglutinin antibody was used at 5 $\mu$g/ml, and the fluorescein isothiocyanate-conjugated secondary antibody was used at a 1:50 dilution. All incubations were carried out on ice.

*Chemotaxis Assay*—Assays of chemotactic responsiveness were performed using ChemoTx™ plates (Receptor Technologies Ltd., Oxon, UK) as described previously (19). Briefly, different concentrations of CCL3 in the presence or absence of a fixed concentration of BX 471 were loaded onto the bottom wells in a final volume of 31 $\mu$l of chemotaxis media (HEPES-modified RPMI 1640 media containing 0.1% bovine serum albumin). The 5-$\mu$m pore filter was placed on top of the wells, and $2 \times 10^5$ cells in a volume of 20 $\mu$l of chemotaxis media were loaded onto the filter. Following incubation for 5 h in a humidified chamber at 37 °C with 5% $CO_2$, the numbers of cells migrating into the well were counted using a hemocytometer. In a primary screen, the ability of BX 471 to inhibit 10 nM CCL3-induced cell migration in all of the point mutants was assessed at least three times in triplicate. Mutants of interest were further characterized over a greater concentration range of CCL3. In every experiment, cells transiently expressing the wild-type CCR1 construct were employed as a positive control.

*$^{125}$I-BX 691 Binding Studies*—Binding assays were performed utilizing scintillation proximity assay (SPA) technology as previously described (9). HEK293 cells expressing human CCR1 at 20,000 cells or human monocytes at 125,000 cells per assay point were used as the receptor source. Cells were incubated with 0.1 nM of $^{125}$I-BX 691 and 0.05–0.1 mg of WGA-PVT-SPA beads at room temperature for 1 h. The receptor-bound $^{125}$I-BX 691 excited the scintillant embedded in the beads and triggered a signal that could be detected by scintillation counter (Wallac microbeta). Nonspecific binding was determined in the presence of 100 nM unlabeled BX 691.

*$^{125}$I-CCL3 Binding Studies of CCR1 Mutants*—Whole cell binding assays on transiently transfected L1.2 cells were performed as described previously (21), using 0.05 nM radiolabeled CCL3 and increasing concentrations of unlabeled competitor. In all experiments, each data point was assayed in triplicate. Data are presented as the percentage of counts obtained in the absence of cold competing ligand. The binding data were curve fitted with the computer program IGOR (Wavemetrics) to determine the affinity and number of sites.

*MembStruk Structure Prediction Method*—The MembStruk3.5 procedure described previously was used to predict the structure of CCR1 (17). The transmembrane regions and the hydrophobic maxima (shown below in bold font and underlined) were predicted using the TM2ndS method with multiple sequence alignment that includes all chemokine receptor sequences. The predicted TM regions were: TM1, QLLPPLYSLVFVIGL**V**GNILVVLVLVQYK; TM2, SIYLLNLAISD**L**LFLFTLPFWIDYKLK; TM3, AMCKILSGFYYTGLY**S**EIFFIILLTIDRYLAIVH; TM4, TFGVITSIIIWAL**A**ILASMPGLYF; TM5, ALKLNLFGLVLPL**L**VMIICYTGII; TM6, RLIFVIMIIFFL**F**WTPYNLTILISVFQDF; and TM7, TEVIAYTHC**C**VNPVIYAFVGER.

Subsequent optimization of the relative translation, rotational orientation, and the kinks and bends of the transmembrane helices were performed as described previously (15). Alternate well packed low energy rotational orientations were also generated as described previously (22). The rotational angle scanning for helix7 was performed by protonating His-293 due to the proximity of Glu-120 on helix3. Extra- and intracellular loops were added using Modeler6v2, and the second extracellular loop was optimized as described previously (22). The resulting structure has the following interhelical hydrogen bonds. Asp-80(TM2) makes a 2.9-Å hydrogen bond with Asn-297(TM7). Asn-52(TM1) makes a 2.1-Å hydrogen bond with Asp-80(TM2). These hydrogen bonds are between the most conserved residues in the class A rhodopsin-like GPCRs. There is also a 2.9-Å hydrogen bond between Asn-297(TM7) and Glu-120(TM3). Glu-120(TM3) also makes a hydrogen bond with His-293 on helix 7. There is a weak or perhaps a water-mediated hydrogen bond between Asn-75(TM2) and Trp-158(TM4) and between Ser-79(TM2) and Ser-119(TM3).

*Prediction of the Binding Site for BX 471*—The void space in the entire receptor structure was divided into 14 regions of $7 \times 7 \times 7$ Å$^3$ volume, and HierDock calculations were performed (3) to determine the binding site of BX 471. Using quantum mechanical calculations, the p$K_a$ of BX 471 was calculated to be neutral at normal pH. BX 471 was subsequently docked into this binding region using the HierDock procedure with protein-movable optimization (3). Subsequent to docking the binding energies were calculated as, BE = PE (ligand in fixed

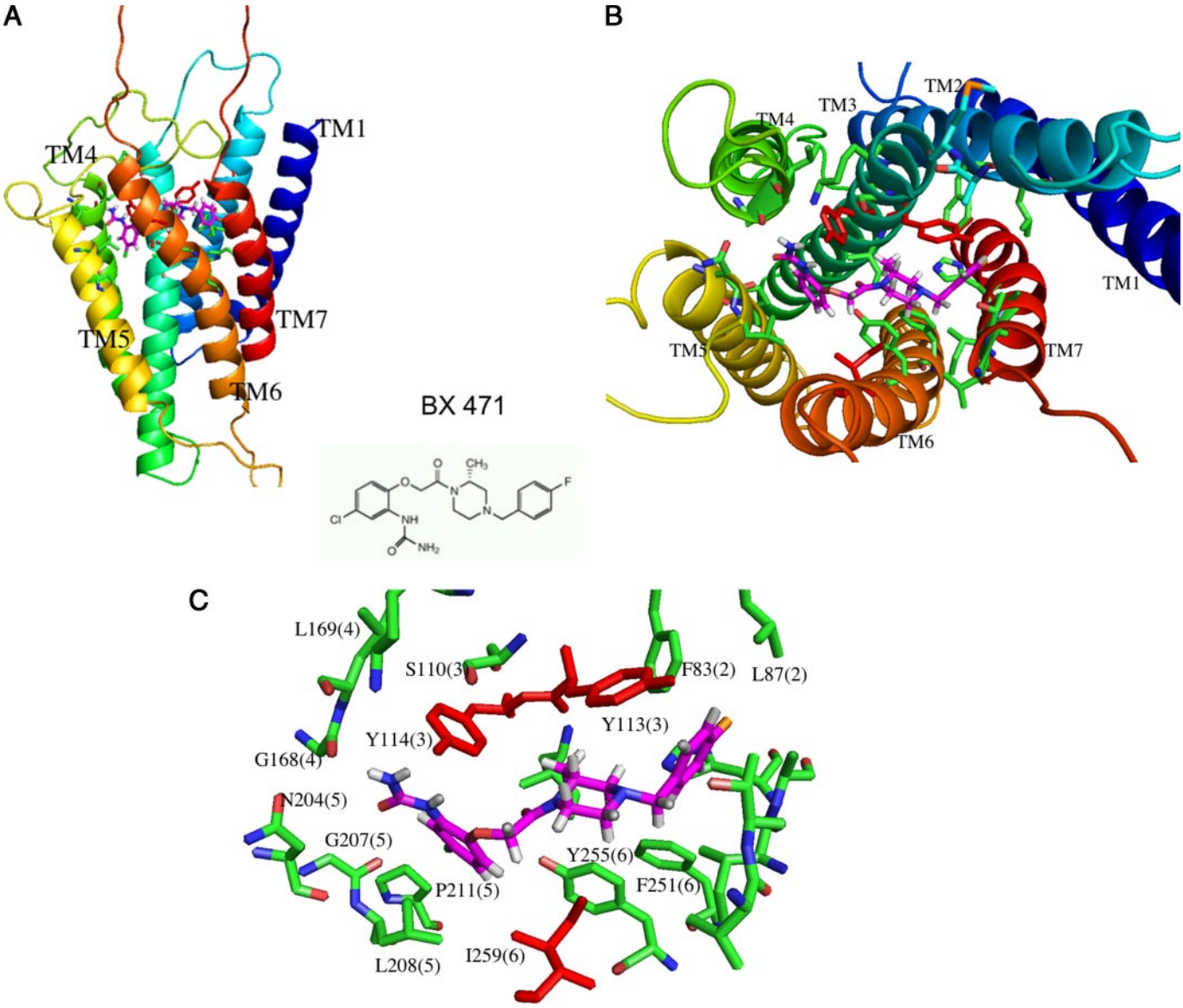


FIGURE 1. **The structure of human CCR1 predicted using MembStruk showing the BX 471 antagonist binding site predicted using HierDock.** *A*, a side view with the extracellular region at the top. *B*, a top view of the predicted structure of BX 471 in the CCR1 binding pocket. The residues shown in *red* (Tyr-113, Tyr-114, and Ile-259) are responsible for anchoring the ligand in this cavity. *C*, details of the predicted binding site (top view), showing all residues within 5Å for the BX 471 ligand. Here, *red* indicates the residues contributing most to the binding.

protein) − PE (ligand in solvation), where BE is the binding energy, PE (ligand in fixed protein) is the potential energy of the ligand calculated with the protein atoms fixed, and PE (ligand in solvation) is the potential energy of the ligand calculated with the analytical volume-generalized Born continuum solvation method. The docked structure with the best binding energy was selected for analysis and molecular dynamics simulations.

*Virtual Screen*—Using GOLD 2.1 (23), we docked all compounds of a filtered version of the Maybridge data base spiked with 35 known CCR1 antagonists from our in-house optimization project and kept the top 50 conformations for each compound. The docked configurations were scored by the sum of the van der Waals and Coulomb protein-ligand interaction energies, using Dock 4.0.1 (24). The top scoring 50% of compounds were further optimized in a 50-conjugate gradient step minimization, using the Universal 1.0.2 force field as implemented in Cerius2. The five lowest energy structures are further minimized for 250 steps. Note that all minimizations are performed in fixed protein. Finally, we calculate the desolvation penalty for the best configuration of each compound using the generalized Born solvation method as implemented in-house (25). Our final score is the sum of Coulomb, van der Waals, and desolvation energies.

## RESULTS AND DISCUSSION

The predicted structure for CCR1 is shown in Fig. 1, along with the binding site of BX 471 that is located between TMs 3, 4, 5, 6, and 7. The strongest protein-ligand interactions in the predicted structure are predominantly of hydrophobic character. They arise from Tyr-113(TM3) and Ile-259(TM6), which anchor the piperazine ring, and Tyr-114(TM3), which provides pi-stacking interactions to the adjacent phenyl ring with the

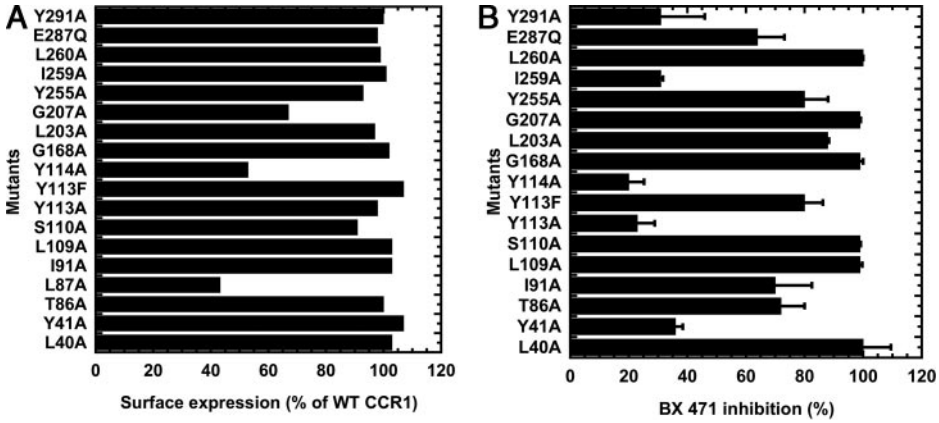


FIGURE 2. **Receptor expression and screening of the ability of BX 471 to inhibit CCL3-induced migration of CCR1 point mutants.** *A*, cell surface expression of CCR1 point mutants. Each of the HA-tagged CCR1 point mutant constructs was transiently transfected independently into L1.2 cells as previously described (18). Twenty-four hours after transfection, cells were incubated with anti-HA antibody, and cell surface expression was analyzed by flow cytometry. Surface expression is shown as a percentage of the expression observed for cells simultaneously transfected with the wild-type CCR1 construct. Data are representative of a typical experiment of at least two independent experiments. *B*, the ability of BX 471 to inhibit CCL3-induced chemotactic responses of L1.2 cells transiently expressing the CCR1 point mutants. The panel of CCR1 mutants was tested for the ability to migrate in response to 10 nM CCL3 in the presence or absence of 100 nM of BX 471. The percentage inhibition was calculated using this equation: % inhibition = 100 − ((the number of cells migrating in the presence of the agonist ÷ the number of cells migrating in the absence of the antagonist) × 100). Where no chemotaxis was observed in the presence of the antagonist, inhibition was described as 100%. Data are shown as % inhibition of chemotaxis by BX 471 ± S.E. from three independent experiments.

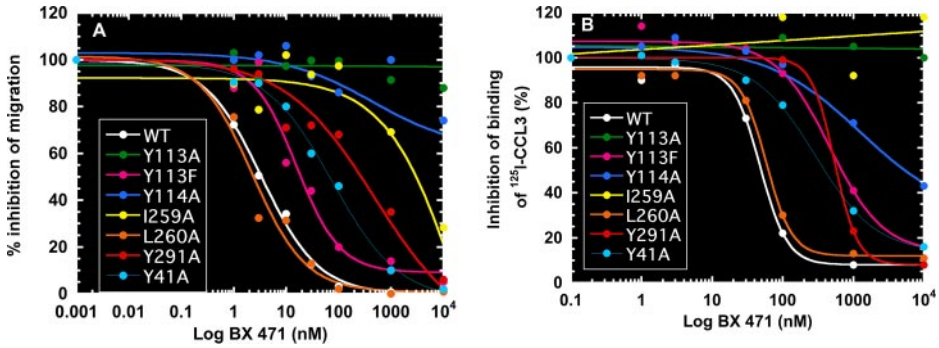


FIGURE 3. **BX 471 inhibition of CCL3-mediated chemotaxis and radiolabeled CCL3 binding to L1.2 cells transiently expressing selected CCR1 point mutants.** *A*, dose-response curves of BX 471 inhibition of CCL3-induced chemotactic responses of L1.2 cells transiently expressing selected CCR1 point mutants. The inhibition of the responses of each construct to a 10 nM concentration of CCL3 is illustrated. Data are representative of a typical experiment of at least two independent experiments. *B*, dose-response curves of BX 471 inhibition of radiolabeled CCL3 binding to L1.2 cells transiently expressing selected CCR1 point mutants. Data are representative of a typical experiment of at least two independent experiments.

urea group (*red* residues in Fig. 1, *B* and *C*). Neither tyrosine forms strong hydrogen bonds to BX 471. The fluorine on BX 471 interacts favorably with one of the methyl groups of Leu-87 and with the phenyl ring of Phe-83. The urea group of BX 471 does not make tight polar interactions with the protein, although it can hydrogen-bond to the carbonyl group of the Gly-168 backbone or the OH-group of Tyr-114. The structure activity relationship from our medicinal chemistry optimization program for this particular substituent indicates that it is not an important site for protein-ligand interactions, because many different substituents of different sizes and polarities are tolerated in this position. Molecular dynamics simulations of the CCR1/BX 471 complex in explicit lipid bilayer and water indicate that this group is highly flexible and forms hydrogen bonds with water molecules that enter the binding region. Molecular dynamics simulation shows that the CCR1 structure with BX 471 bound is stable over the entire 10 ns of simulation time. Because the prediction of the loop structures is associated with a large degree of uncertainty, we ignored the contribution of residues in the loop to binding.

To verify the predicted binding site of BX 471, we constructed a series of 17 receptor mutants (Fig. 2). These mutants included key residues predicted to be in the binding pocket for BX 471 (Tyr-113, Tyr-114, and Ile-259) together with residues Tyr-41, Glu-287, and Tyr-291, identified as playing a role in antagonist binding in previous studies with charged CCR1 antagonists (18, 26). Cells separately transfected with either wild-type CCR1 or with point mutants of CCR1 predicted to be outside the antagonist binding site were included as controls (Fig. 2). The point mutants were all transiently expressed at high levels on the surface of L1.2 cells as detected by flow cytometry after incubation with an antibody to an epitope tag at the receptor amino terminus (Fig. 2*A*). The CCR1 point mutants were then screened for antagonism by BX 471 of chemotactic responses to 10 nM CCL3 (Fig. 2*B*). Several mutants, including Y41A, Y113A, Y114A, I259A, and Y291A were very resistant to inhibition by BX 471, and full dose-response curves for these and other selected mutants were carried out. The functional assays revealed that BX 471 has an $IC_{50}$ greater than 10 $\mu$M for inhibition of chemotaxis in the Y113A, Y114A, and I259A mutants (Fig. 3*A* and Table 1), as expected from the model. Other mutants, including Y41A and Y291A, were also resistant to inhibition of chemotaxis by BX 471 (Fig. 3*A* and Table 1), consistent with the predictions.

The CCR1 point mutants were next tested for the ability of BX 471 to displace the specific binding of $^{125}$I-CCL3 to the wild-type and mutant receptors (Fig. 3*B* and Table 1). Competition binding assays revealed that the mutations Y113A and Y114A on TM3 and I259A on TM6 resulted in a significant reduction in binding of BX 471, in line with the data from the chemotaxis assays. Specifically, whereas the antagonist binds to the wild-type receptor with an $IC_{50}$ of 10 nM, the $IC_{50}$ for the Y113A and I259A mutants is >10 $\mu$M, and for Y114A it is >5 $\mu$M. The large effects of these three mutations on BX 471 binding had been predicted in the computational mutation studies that showed a change in binding energy of 6.28, 5.79, and 9.24 kcal/mol, respectively, for these three mutants (Table 1). The large decrease in binding energy predicted for Y113A, Y114A,

and I259A arises predominantly from the loss of favorable van der Waals interactions of the phenyl containing residues with the piperazine ring in BX 471. Indeed, the calculations followed by experiments show that replacement of Tyr-113 by phenylalanine (Y113F) has a minimal effect on the ability of BX 471 to inhibit binding or chemotaxis, compared with a total inability of the antagonist to inhibit either process in the Y113A mutant (see Fig. 3 and Table 1).

Interestingly the residues Tyr-41, Glu-287, and Tyr-291, which were identified to bind to the protonated antagonist UCB35625 (18), and Glu-287, which has also been implicated in the binding of another protonated antagonist, BX 510 (26), are not part of the binding pocket for BX 471 even though we do observe changes in experimental binding and activation studies with these mutants. Y41A(TM1) makes a strong (2.85 Å) interhelical hydrogen bond to Glu-287(TM7), which is well preserved during the molecular dynamics simulations in explicit water and lipid with antagonist bound. Tyr-291(TM7) is one turn below Glu-287(TM7) and has a loose aromatic stacking interaction with Tyr-41(TM1). We speculate that this network of hydrogen bonding between Tyr-41 and Glu-287 combined with aromatic stacking between Tyr-41 and Tyr-291 is important for structural stability, and therefore mutation of any of these residues affects both binding and activation of CCR1. In contrast, these residues play only a minor role in binding the neutral antagonist BX 471, where Tyr-113, Tyr-114, and Ile-259 play the most important role. Thus, the binding site of the neutral antagonist BX 471 is shifted toward helices 3, 6, and 7 compared with the binding site of protonated antagonists that lies closer to helices 1 and 2.

**TABLE 1**

**Summary of experiments on the effect of CCR1 mutations on BX 471 inhibition of CCL3-induced receptor binding and chemotaxis**

Changes in binding energies are calculated as the difference in binding energy of BX 471 to the wild-type receptor compared with binding to the mutant receptor. Binding energy = potential energy of ligand (in protein) − potential energy of ligand (in solvent). Binding energies are reported in kcal/mol, and a more positive number indicates a decrease in affinity of the antagonist for the receptor.

| Mutant | $IC_{50}$ BX 471 inhibit binding | Ratio | Calculated change in BE |
|---|---|---|---|
| | nM | | |
| Wild type | 10 ± 5 | 1 | 0.0 |
| Y113A | >10,000 | >1,000 | 6.28 |
| I259A | >10,000 | >1,000 | 5.79 |
| Y114A | 5,017 ± 1970 | 502 | 9.24 |
| I91A | 849 ± 287 | 85 | −0.55 |
| Y291A | 542 ± 308 | 54 | 0.04 |
| Y113F | 464 ± 164 | 46 | 1.49 |
| T86A | 348 ± 180 | 35 | −0.52 |
| E287Q | 344 ± 122 | 34 | 0.06 |
| Y41A | 264 ± 179 | 26 | 0.02 |
| L260A | 58 ± 6 | 6 | 0.03 |
| **Mutant** | **$IC_{50}$ BX 471 inhibit migration** | **Ratio** | |
| | nM | | |
| Wild type | 3.4 ± 0.54 | 1 | |
| Y113A | >10,000 | >2,941 | |
| Y114A | >10,000 | >2,941 | |
| I259A | >10,000 | >2,941 | |
| Y41A | 541 ± 54 | 159 | |
| Y291A | 491 ± 70 | 144 | |
| E287Q | 284 ± 102 | 83 | |
| I91A | 233 ± 73 | 68 | |
| T86A | 77.9 ± 34 | 23 | |
| Y113F | 16 ± 6 | 5 | |
| L260A | 2.3 ± 0.88 | 1 | |

A major assumption in receptor mutagenesis studies is that any loss of function observed is due to the mutation alone and does not involve structural changes in the molecule. Such an assumption is generally valid for surface residues but is not necessarily true for buried/structural large hydrophobic or aromatic residues. Because the residues we have identified as important for binding in this study, Tyr-113, Tyr-114, and Ile-259, are buried hydrophobic or aromatic residues, it was important to determine that the mutations did not perturb the structure and function of the receptor. To test the structural integrity of the three CCR1 mutants Y113A, Y114A, and I259A we carried out both displacement binding and chemotaxis studies with the CCR1 ligand CCL3. The binding studies revealed (Fig. 4*B*) that all three mutants had very similar affinities for binding of CCL3 (WT $K_i$ = 31.8 ± 16.1 nM; Y113A $K_i$ = 22.3 ± 3.1 nM; Y114A $K_i$ = 15.3 ± 3.3 nM; I259A $K_i$ = 14.7 ± 4.9 nM). In addition all three mutants responded chemotactically in a similar dose-responsive manner as wild-type CCR1 to increasing concentrations of CCL3 (Fig. 4*A*). These data strongly suggest that the structural integrity of these mutants with respect to chemokine binding and activation is not altered.

We cannot rule out, however, that structural changes have occurred in these mutants that would not be manifested by changes in chemokine function. We do think that this is unlikely, however, for several reasons. First, we see robust expression of the CCR1 mutants compared with wild-type CCR1, and misfolded proteins would tend to exhibit lower expression. Second, in the apo-protein structure of CCR1 (after 10 ns of molecular dynamics simulation in explicit lipid bilayer and water), Tyr-113(TM3) has favorable van der Waals interactions with Ile-259(TM6) and hydrogen bond interaction with Thr-286(TM7). Tyr-114

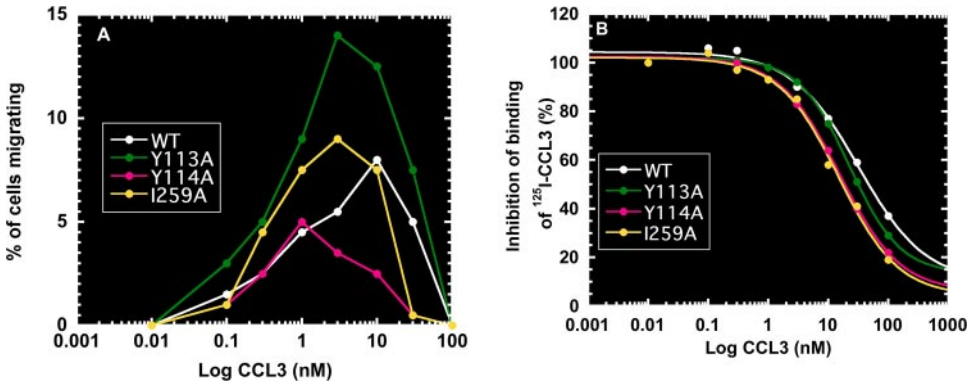


FIGURE 4. **CCL3 inhibition of CCL3-mediated chemotaxis and radiolabeled CCL3 binding to L1.2 cells transiently expressing selected CCR1 point mutants.** *A*, dose-response curves of CCL3-induced chemotactic responses of L1.2 cells transiently expressing selected CCR1 point mutants. Data are representative of a typical experiment of at least two independent experiments. *B*, dose-response curves of CCL3 inhibition of radiolabeled CCL3 binding to L1.2 cells transiently expressing selected CCR1 point mutants. Data are representative of a typical experiment of at least two independent experiments.

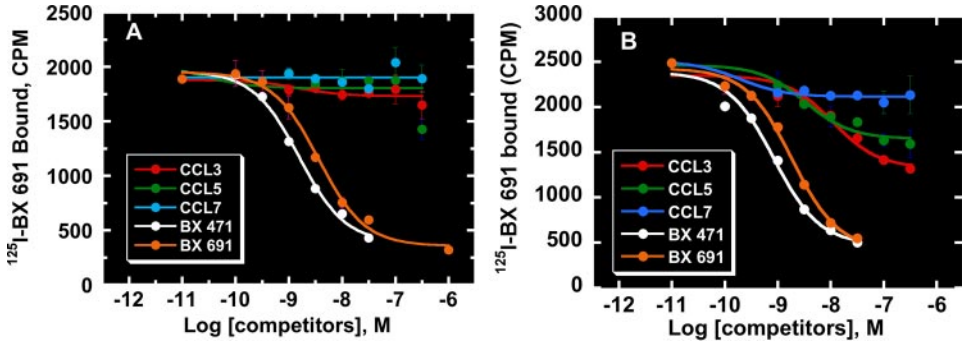


FIGURE 5. **Inhibition of $^{125}$I-BX 691 binding to human CCR1 by unlabeled antagonists and agonists on HEK293 cells stably expressing CCR1 (*A*) and human monocytes (*B*).** Cells were incubated for 60 min at room temperature with $^{125}$I-BX 691 in the presence of increasing concentrations of compounds or chemokines. The bound $^{125}$I-BX 691 was determined using SPA technology. Nonspecific binding was defined as the binding in the presence of 1 $\mu$M of unlabeled BX 691. Data are shown as total binding ± S.E. from three independent experiments.

**TABLE 2**

**Correlation between the calculated change in binding energies (BE) and experimental binding affinities for human CCR1 docked with CCR1 antagonists**

The structures of a few CCR1 antagonists are shown. The calculated change in binding energies for the second compound in each table is relative to the first compound in each table, which has a normalized reference energy of 0.0 kcal/mol. A positive change in BE indicates lower affinity of the antagonist for the receptor.

(A)

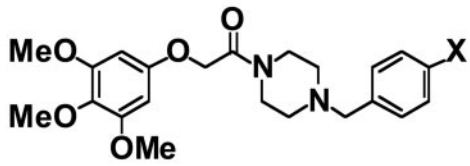

| Cmpd | X | $IC_{50}$ (nM) | Calculated change in binding energy (kcal/mol) |
|---|---|---|---|
| BX 758 | F | 20 | 0.0 |
| BX 937 | OMe | >10,000 | 3.1 |

(B)

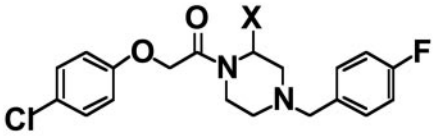

| Cmpd | X | $IC_{50}$ (nM) | Calculated change in binding energy (kcal/mol) |
|---|---|---|---|
| BX 474 | Me | 10 | 0.0 |
| BX 332 | $CH_2NH$ Me | >10,000 | 12.3 |

on TM3 has weak van der Waals interactions with Val-263(TM6) and Tyr-113(TM3). Ile-259 makes van der Waals contact with Leu-208(TM4) and Val-263(TM6). In the Y113A mutant, the loss of hydrogen bond interaction with Thr-286 is partially compensated for by the favorable interaction of the methyl group of Ala-113 with the methyl group of Thr-286(TM7). We speculate that this hydrogen bond is not a critical structural factor, because mutating Tyr-113 → Ala or Tyr-113 → Phe did not affect the cell surface expression levels of these mutants. Y114A and I259A mutants similarly have weaker van der Waals interactions that may not impair the folding of the receptor. Based on these observations along with the robust level of cell surface expression seen for these mutant receptors, we speculate that mutation of these residues to Ala does not affect the structural integrity of the receptor. This validates our contention that they play a key role in ligand binding of the antagonist BX 471.

The chemokine receptor antagonist BX 471 is highly specific for CCR1. Previous work has shown that it has no cross-reactivity at concentrations >10 $\mu$M with 30 other GPCRs, including several chemokine receptors (9). The only exception is the low affinity binding to CCR3 with a $K_i$ of 1.4 $\mu$M. CCR3 has 63% sequence identity to CCR1, and the residues Tyr-113, Ile-259, Ile-91, and Tyr-291 are conserved between the two receptors. Based on our model we speculate that the basis for the low affinity binding of BX 471 to CCR3 is partly due to the conservation of residues Tyr-113 and Ile-259 in CCR3 that have been shown to be important in the binding of BX 471 to CCR1.

To further characterize the CCR1 antagonist binding site we utilized a $^{125}$I-labeled CCR1 antagonist generated by replacing the chloro-group on the benzyl ring of BX 471 with an iodo-group. The resulting compound BX 691 is a functional antagonist for CCR1 with similar potency ($K_i$ 1.7 nM). Because BX 471 and BX 691 behave similarly as CCR1 antagonists, $^{125}$I-BX 691 was used to characterize the direct interaction of small molecule CCR1 antagonists with CCR1. $^{125}$I-BX 691 binds to CCR1 on human monocytes as well as on HEK293 cells that express the receptor (Fig. 5). The binding is dose-responsively inhibited by unlabeled BX 471 and BX 691, with affinities similar to those for displacing $^{125}$I-CCL3 binding (Fig. 5). However, the CCR1 agonists CCL3, CCL5, and CCL7 failed to displace $^{125}$I-BX 691 binding to CCR1, suggesting that they do not bind to the same site on the receptor as the antagonists. These data clearly suggest that BX 471 and BX 691 are allosteric antagonists of CCR1 and bind to sites on the receptor that are non-overlapping and distinct from the agonist binding site. Indeed, structure-function studies have revealed that chemokines such as CCL3 bind to CCR1 via residues in the N terminus and in the extracellular loops (27, 28). In contrast, we have shown here that BX 471, like other chemokine receptor antagonists (29, 30), binds to CCR1 in the transmembrane domain, similar to the transmembrane binding domain of 11-*cis*-retinal in rhodopsin. Through its interaction with residues in the transmembrane domain, BX 471 induces a conformational change in the receptor that leads

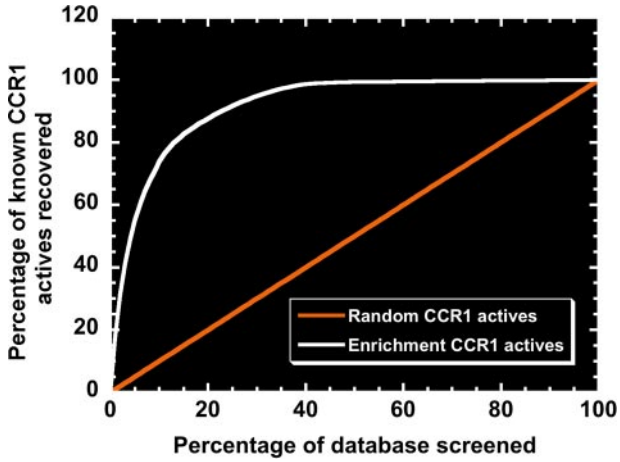


FIGURE 6. **Virtual ligand screening using the predicted binding site of BX 471.** A filtered version of the Maybridge data base (~52,000 compounds), enriched with 35 known CCR1 antagonists (many that are not related to BX 471) ranging in affinity between 1 and 1000 nM, was docked into the predicted CCR1 structure using a hierarchical virtual ligand screening procedure as described under "Experimental Procedures." The figure shows the percentage (*white*) of CCR1 actives recovered compared with the percentage of random CCR1 actives recovered (*orange*) as a percentage of the data base screened.

to displacement of bound chemokine from its extracellular binding site. In contrast, when radiolabeled BX 471 is bound, CCR1 agonists are unable to competitively displace the antagonist.

To further validate the predicted structure and binding site, we docked several antagonists, belonging to the same piperazine template as BX 471, to CCR1 (Table 2). The model clearly distinguishes strong from weak binders according to their calculated binding energies. Thus, we believe that structure-based design using GPCR models can be used in future projects during the medicinal chemistry optimization phase of lead compounds.

Lastly, we performed a retrospective virtual ligand screen using the predicted structure and binding site of BX 471 to explore if the model could be used in the lead identification process. To this end, we docked a filtered version of the Maybridge data base (~51,000 compounds) enriched with 35 known CCR1 antagonists ranging in affinity between 1 and 1000 nM, which represent four different chemical templates (some representative structures are shown in Table 2) into the predicted structure without loops. We used a hierarchical virtual ligand screen procedure as described under "Experimental Procedures." The results of the virtual screen showed that 43% of all CCR1 actives were recovered in the top 2% of screened molecules and 63% of the known CCR1 antagonists scored within the top 5% of the screened molecules (Fig. 6). This corresponds to a hit enrichment of 21 times over random at 2% and 13 times over random at 5% of the data base screened, where enrichment factors have been calculated as in a previous study (11). These data demonstrate that predicted GPCR structures are useful in a structure-based *in silico* drug discovery process and underscore the ability of the CCR1 model to retrieve seeded CCR1 antagonists from multiple templates with high efficiency from a chemical data base. This is important, because it validates the model in addition to the validation provided by the experimentally determined binding and activation data described earlier. The next logical step in this process will be to utilize the model in a prospective virtual screen to identify new CCR1 actives from commercially available chemical databases. Hopefully this will aid and abet the drug discovery process by finding new lead compounds to supplement traditional approaches that utilize high throughput screening of compound libraries.

In conclusion, we predicted a structure of the human chemokine receptor CCR1 using the MembStruk computational method. Additionally, we predicted the binding site of the neutral antagonist BX 471 in CCR1 using the HierDock computational method. The structure suggested that the residues Tyr-113, Tyr-114, and Ile-259 are the most important for binding of the antagonist BX 471 to CCR1. We then validated the predicted antagonist binding site in CCR1 using mutational analysis. Further, we used the protein structure to successfully identify CCR1 antagonists in a retrospective virtual ligand screen of a large data base, demonstrating the utility of structure-based *in silico* methods in the hit-finding process of GPCR antagonists. Our results suggest that structure-based *in silico* rational drug design for GPCR targets is feasible.

## REFERENCES


1. Nollert, P., and Stewart, L. (2004) *Drug Discov. Today Targets* **4,** 2–4
2. Horuk, R. (2001) *Growth Factor Rev.* **12,** 313–335
3. Vaidehi, N., Floriano, W. B., Trabanino, R., Hall, S. E., Freddolino, P., Choi, E. J., Zamanakos, G., and Goddard, W. A., III. (2002) *Proc. Natl. Acad. Sci. U. S. A.* **99,** 12622–12627
4. Ribeiro, S., and Horuk, R. (2005) *Pharmacol. Ther.* **107,** 44–58
5. Baggiolini, M. (1998) *Nature* **392,** 565–568
6. Neote, K., DiGregorio, D., Mak, J. Y., Horuk, R., and Schall, T. J. (1993) *Cell* **72,** 415–425
7. Gao, J. L., Kuhns, D. B., Tiffany, H. L., McDermott, D., Li, X., Francke, U., and Murphy, P. M. (1993) *J. Exp. Med.* **177,** 1421–1427
8. Pease, J. E., and Horuk, R. (2005) *Exp. Opin. Investig. Drugs* **14,** 785–796
9. Liang, M., Mallari, C., Rosser, M., Ng, H. P., May, K., Monahan, S., Bauman, J. G., Islam, I., Ghannam, A., Buckman, B., Shaw, K., Wei, G. P., Xu, W., Zhao, Z., Ho, E., Shen, J., Oanh, H., Subramanyam, B., Vergona, R., Taub, D., Dunning, L., Harvey, S., Snider, R. M., Hesselgesser, J., Morrissey, M. M., and Perez, H. D. (2000) *J. Biol. Chem.* **275,** 19000–19008
10. Palczewski, K., Kumasaka, T., Hori, T., Behnke, C. A., Motoshima, H., Fox, B. A., Le Trong, I., Teller, D. C., Okada, T., Stenkamp, R. E., Yamamoto, M., and Miyano, M. (2000) *Science* **289,** 739–745
11. Shacham, S., Marantz, Y., Bar-Haim, S., Kalid, O., Warshaviak, D., Avisar, N., Inbal, B., Heifetz, A., Fichman, M., Topf, M., Naor, Z., Noiman, S., and Becker, O. M. (2004) *Proteins* **57,** 51–86
12. Bissantz, C., Bernard, P., Hibert, M., and Rognan, D. (2003) *Proteins* **50,** 5–25
13. Bissantz, C., Logean, A., and Rognan, D. (2004) *J. Chem. Inf. Comput. Sci.* **44,** 1162–1176
14. Moro, S., Spalluto, G., and Jacobson, K. A. (2005) *Trends Pharmacol. Sci.* **26,** 44–51
15. Trabanino, R. J., Hall, S. E., Vaidehi, N., Floriano, W. B., Kam, V. W., and Goddard, W. A., 3rd. (2004) *Biophys. J.* **86,** 1904–1921
16. Freddolino, P. L., Kalani, M. Y., Vaidehi, N., Floriano, W. B., Hall, S. E., Trabanino, R. J., Kam, V. W., and Goddard, W. A., III. (2004) *Proc. Natl. Acad. Sci. U. S. A.* **101,** 2736–2741
17. Kalani, M. Y., Vaidehi, N., Hall, S. E., Trabanino, R. J., Freddolino, P. L., Kalani, M. A., Floriano, W. B., Kam, V. W., and Goddard, W. A., III. (2004) *Proc. Natl. Acad. Sci. U. S. A.* **101,** 3815–3820
18. de Mendonca, F. L., da Fonseca, P. C., Phillips, R. M., Saldanha, J. W., Williams, T. J., and Pease, J. E. (2005) *J. Biol. Chem.* **280,** 4808–4816
19. Martinelli, R., Sabroe, I., LaRosa, G., Williams, T. J., and Pease, J. E. (2001)

*J. Biol. Chem.* **276,** 42957–42964
20. Auger, G. A., Pease, J. E., Shen, X., Xanthou, G., and Barker, M. D. (2002) *Eur. J. Immunol.* **32,** 1052–1058
21. Hesselgesser, J., Ng, H. P., Liang, M., Zheng, W., May, K., Bauman, J. G., Monahan, S., Islam, I., Wei, G. P., Ghannam, A., Taub, D. D., Rosser, M., Snider, R. M., Morrissey, M. M., Perez, H. D., and Horuk, R. (1998) *J. Biol. Chem.* **273,** 15687–15692
22. Trabanino, R. J. (2004) *Prediction of Structure, Function, and Spectroscopic Properties of G-protein-coupled Receptors: Methods and Applications.* Ph.D. thesis, California Institute of Technology
23. Evers, A., and Klabunde, T. (2005) *J. Med. Chem.* **48,** 1088–1097
24. Floriano, W. B., Vaidehi, N., Zamanakos, G., and Goddard, W. A., III. (2004) *J. Med. Chem.* **47,** 56–71
25. Still, W. C., Tempczyk, A., Hawley, R. C., and Hendrickson, T. (1990) *J. Am. Chem. Soc.* **112,** 6127–6129
26. Onuffer, J., McCarrick, M. A., Dunning, L., Liang, M., Rosser, M., Wei, G. P., Ng, H., and Horuk, R. (2003) *J. Immunol.* **170,** 1910–1916
27. Pease, J. E., Wang, J., Ponath, P. D., and Murphy, P. M. (1998) *J. Biol. Chem.* **273,** 19972–19976
28. Zoffmann, S., Chollet, A., and Galzi, J. L. (2002) *Mol. Pharmacol.* **62,** 729–736
29. Mirzadegan, T., Diehl, F., Ebi, B., Bhakta, S., Polsky, I., McCarley, D., Mulkins, M., Weatherhead, G. S., Lapierre, J. M., Dankwardt, J., Morgans, D., Jr., Wilhelm, R., and Jarnagin, K. (2000) *J. Biol. Chem.* **275,** 25562–25571
30. Dragic, T., Trkola, A., Thompson, D. A., Cormier, E. G., Kajumo, F. A., Maxwell, E., Lin, S. W., Ying, W., Smith, S. O., Sakmar, T. P., and Moore, J. P. (2000) *Proc. Natl. Acad. Sci. U. S. A.* **97,** 5639–5644